

Improved Multi-Path Interference Separation for Indirect 3D Time-of-Flight using Particle Swarm Optimization

Matthias Ludwig¹, Jonas Gutknecht¹ and Teddy Loeliger

Institute of Signal Processing and Wireless Communications

ZHAW Zurich University of Applied Sciences

Winterthur, Switzerland

Email: matthiasandreas.ludwig@zhaw.ch

Abstract—The accuracy of indirect 3D Time-of-Flight (3D ToF) measurements is often limited by multi-path interferences (MPI) caused by multi-layer ToF conditions. Taking multiple measurements of the same scene at different modulation frequencies allows separating the interfering signal components of the individual paths according to several optimization methods described in literature. Orthogonal matching pursuit (OMP) optimization has been reported to achieve good path separation performance and superior results compared to particle swarm optimization (PSO). This work presents improved PSO performance for MPI separation based on new experimental data and refined PSO strategy. The current PSO approach achieves good distance separation in the setup used with low RMS distance errors in the order of 20 cm in situations where the OMP approach shows RMS errors higher than 100 cm. The previously reported minimum distance difference limitation between two separate objects of 2.7 m for the OMP algorithm could be reduced to roughly 0.75 m for the PSO algorithm. The trade-off between image accuracy and computing effort is explored and presented with respect to PSO parameter settings.

Index Terms—3D Time-of-Flight (3D ToF), Multi-Path Interference (MPI), Multi-Layer ToF, Orthogonal Matching Pursuit (OMP), Particle Swarm Optimization (PSO)

I. INTRODUCTION

The indirect 3D Time-of-Flight (iToF) measurement method is shown in simplified form in Fig. 1. A light source with modulated light illuminates the objects and the reflected light is demodulated in each pixel of the camera [1], [2]. The phase detection measures the time-of-flight from the light source to the camera and yields the distance of the object in each pixel and thus a 3D point cloud of the scene.

Using a sine wave signal for modulation, the delayed sine wave signal with phase delay φ and relative amplitude a appears in the camera pixel. The signal delay and attenuation

can be modelled as a complex vector for the demodulated signal m :

$$m = a \cdot \exp(j \cdot \varphi) \quad (1)$$

The phase delay φ of the received signal caused by the time-of-flight results in an object distance of:

$$d = c \cdot \frac{t_{ToF}}{2} = c \cdot \frac{\varphi}{4\pi \cdot f} \quad (2)$$

In many situations, multi-path interference (MPI) occurs and leads to significantly wrong distance data in iToF measurements [3]. MPIs are often caused by sharp edges, semi-transparent layers, mesh structures, mirroring surfaces or stray light. In these cases, multiple signals with different delays and amplitudes may interfere and a superposition signal m of the K multi-path signals is measured and interpreted as a single phase delay φ and amplitude a . To obtain the correct distances d_k of the K individual paths, the different superimposed signals of the multiple paths have to be separated. This can be done by measuring multiple superposition signals m_n at N different modulation frequencies f_n :

$$m_n = \sum_{k=0}^{K-1} a_k \cdot \exp\left(j \cdot \frac{4\pi \cdot f_n}{c} \cdot d_k\right) = a_n \cdot \exp(j \cdot \varphi_n) \quad (3)$$

According to [3], the K individual distances d_k can be extracted from the N different measurements m_n with the closed-form Prony method (CF) [4], Orthogonal Matching Pursuit Optimization (OMP) [5], or Particle Swarm Optimization (PSO), where OMP has been reported to be superior to PSO [3]. This paper demonstrates that this assertion is not valid with proper PSO parameters.

In section II the performance and limitations of the reported OMP method are briefly reviewed. Section III presents the achieved performance improvements using the PSO approach and in section IV the computing effort of a PSO based implementation is analysed. Section V summarizes and concludes this work.

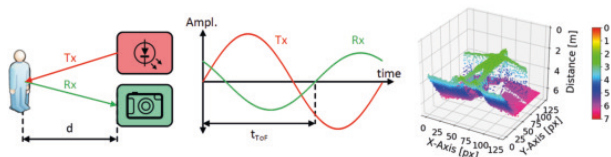


Fig. 1. Indirect 3D ToF camera measurement principle.

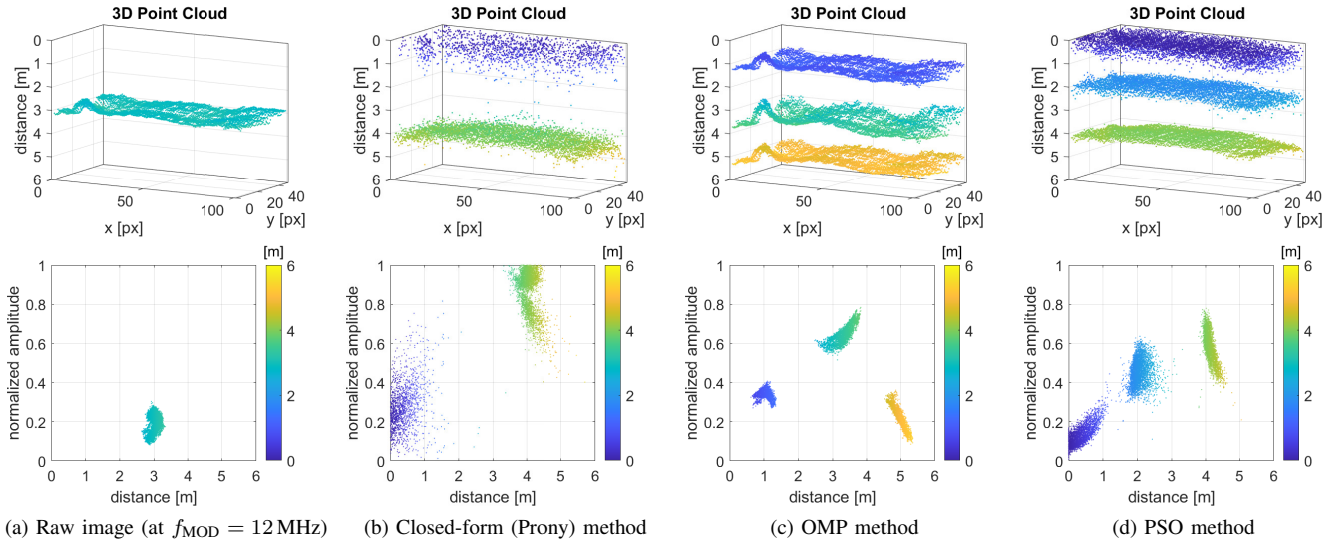


Fig. 2. 3D point cloud with amplitude vs. distance scatter plot of reference scene A according to the different methods.

II. OMP PERFORMANCE AND LIMITATIONS

In [3] it has been shown that OMP optimization can achieve good multi-path separation. However, this optimization strategy implies some severe drawbacks that can drastically limit the accuracy and the minimum distance difference between two objects/paths that can still be separated. The following results have been achieved using an ESPOS DME 660 camera with appropriate distance, amplitude and temperature compensation. 14 modulation frequencies from 10 to 36 MHz in 2 MHz steps have been used. The number of individual paths K is determined based on prior knowledge of the scene. The open research data are available on Zenodo as *3D ToF MPI multi-frequency mesh dataset* [6].

A. Accuracy

Fig. 2 shows the multi-path separation results of the different approaches with regard to scene A that suffers from MPI as shown in Fig. 3. The scene consists of a stray light component from a close object at a distance of about 0.3 m, a semi-transparent mesh at 2 m distance, and a background wall at 4 m. $K = 3$ has been used for the CF, OMP and PSO methods. TABLE I compares the algorithms based on the absolute error of the mean value $\|\mu_e\|$, the distance standard deviation σ_e , the RMS value of the absolute error RMSE, and the experimentally found minimum distance difference Δd_{min} . Due to the MPI, the raw image shows a single, wrong distance of about 3 m in all pixels (Fig. 2a). The CF result can somewhat separate the stray light from the other objects, but the other two components are mixed and the mesh is not visible (Fig. 2b). The OMP approach succeeds in separating stray light, mesh and wall, however all these objects have significantly wrong distances with mean errors in the order of 1 m (Fig. 2c). This behaviour is due to the fact, that in the first step the OMP reproduces the superposition of the strong signal from the mesh and the wall by a single estimated signal, which

leads to a wrong estimated distance in between the mesh and the wall that is neither the mesh nor the wall. In the next steps, the OMP produces signals to compensate for the errors due to the mismatch in the previous steps, which leads to consecutive errors.

The PSO result shows good separation of all three paths including some distance noise with mean errors of about 0.06 m (Fig. 2d).



Fig. 3. Measurement setup similar to scene A

TABLE I
DISTANCE ERROR STATISTICS OF BENCHMARK MEASUREMENT.

Dataset	$\ \mu_e\ $	σ_e	RMSE	Δd_{min}
Raw image	1 m	0.1 m	1 m	
Closed-Form (Prony)	0.5 m	0.7 m	0.9 m	> 4 m
OMP	1 m	0.3 m	1.1 m	≈ 2.7 m
PSO	0.06 m	0.3 m	0.3 m	≈ 0.75 m

B. Minimum Distance Difference

The OMP is apparently capable of separating the objects in scene A, but in fact the mesh and the wall are merged due to the low distance difference between the layers. OMP results are good for distance differences of typically > 2.7 m [3]. Lower differences lead to merged layers and therefore high distance errors.

III. PSO IMPROVEMENTS

The above limitations of the OMP approach can be overcome by using a global optimizer like the PSO and adjusting the parameters and the strategy accordingly. Fig. 2d shows the improved accuracy of the PSO result in scene A with respect to the OMP. Fig. 4 shows the multi-path separation results of both the OMP and the PSO approach with regard to a new scene B that suffers from MPI and features a low distance difference of 1 m. Scene B consists of a semi-transparent mesh at 2 m and a background wall at 3 m. The layers have been separated for both methods with the assumption of two layers ($K = 2$).

The OMP algorithm is unable to separate the two objects, resulting in an incorrect single distance value. The PSO is able to separate the two objects and yields correct distances. The RMS distance error is 13 cm. This shows that the PSO is able to achieve good separation, low distance error, and reduced minimum distance difference of the multiple paths. Similar performance can be attained by reducing the number of frequencies from 14 to 4 uniformly distributed frequencies across the bandwidth for scene B. This speeds up the acquisition and the computing time. Additional research is required to explore the relationship between the number of frequencies, accuracy, and the minimum distance difference between objects.

Fig. 5 shows the improved MPI separation of scene C applied to a toy horse hidden behind a mesh at 2 m distance. The toy horse is at 3.3 m distance in front of a background wall at 5 m. The raw image on the left shows an unreal merged layer at completely wrong distances, while the processed image on the right shows the toy horse in front of the background wall in correct 3D representation. The layers have been separated using PSO with $K = 2$ and the front layers at $d \leq 2.6$ m have been removed from the data to make them invisible. This proves that this method can be used to see semi-transparent layers or virtually see through them using Multi-Layer ToF.

IV. COMPUTING EFFORT

One major advantage of the OMP algorithm is the relative low computing effort in contrast to the PSO. The addition of a subsequent gradient-based optimizer to the PSO allows reducing its complexity, as shown in TABLE II. Adding a

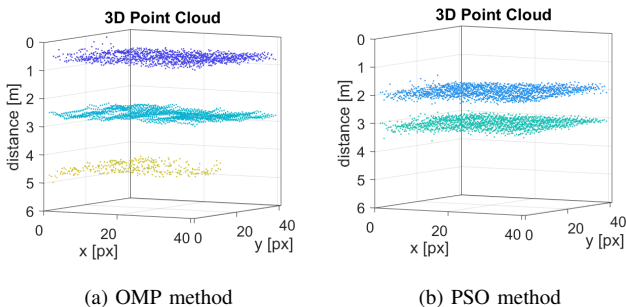
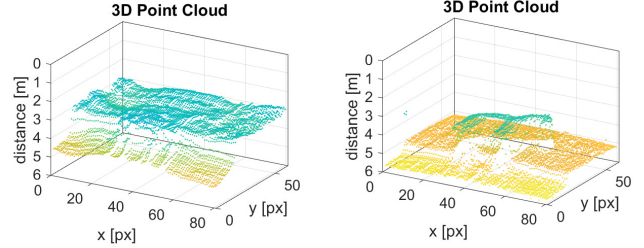


Fig. 4. 3D point cloud with scatter plot of reference scene B according to the OMP and PSO methods.



(a) Raw image (at $f_{\text{MOD}} = 12$ MHz) (b) Processed image (PSO method)

Fig. 5. Scene C: Raw image (a) and processed image with separated multi-paths and removed front layers using PSO (b).

TABLE II
COMPARISON OF COMPUTING EFFORT AND ACCURACY FOR $K = 2$ ON AN I7-8550U AT 3.5GHZ FOR SCENE B.

Swarm size	# iter. of PSO	subsequent optimizer (# iter.)	$\ \mu_e\ $	σ_e	time per pixel
80	295	-	4 cm	11 cm	256 ms
20	90	-	7 cm	29 cm	26 ms
20	39	interior-point (114)	4 cm	10 cm	24 ms
5	5	interior-point (109)	3 cm	9 cm	16 ms
5	5	interior-point (66)	9 cm	15 cm	12 ms

gradient-based optimizer and reducing the swarm size from 80 to 5 and the number of iterations from 295 to 5 results in roughly the same accuracy at much lower computing time for scene B. With this optimized parameter set, PSO is mainly used to find optimal starting points for the subsequent gradient-based optimizer. A gradient-based optimizer on its own is insufficient; it requires appropriate initial values supplied by the PSO.

Significant reduction in computation time can be achieved by parallelizing the algorithm on a GPU and by porting the algorithm from MATLAB to a faster language such as OpenCL.

V. CONCLUSION

The global optimizer approach employing the PSO offers enhanced multi-path interference separation and achieves significantly better accuracy and a lower minimum distance difference limitation than the previously reported sequential OMP approach. The experimental data provided achieved RMS distance errors of approximately 0.2 m and minimum distance differences of around 0.75 m. The efficient combination of a PSO with small swarm size and a subsequent gradient-based optimizer achieves reduced computing effort of typically 10-20 ms per pixel. Efficient parallelized implementations of the algorithm on GPUs are mandatory for real-time applications using the PSO approach.

ACKNOWLEDGMENT

This work has been funded by the Swiss National Science Foundation SNSF (PT00P2_198986).

REFERENCES

- [1] R. Lange, "3D time-of-flight distance measurement with custom solid-state image sensors in CMOS/CCD-technology," Ph.D. dissertation, Universität Siegen, 2000.
- [2] R. Lange and P. Seitz, "Solid-state time-of-flight range camera," *IEEE Journal of Quantum Electronics*, vol. 37, no. 3, pp. 390–397, 2001.
- [3] J. Gutknecht and T. Loeliger, "Multi-Layer ToF: Comparison of different multipath resolve methods for indirect 3D time-of-flight," in *2021 IEEE Sensors*, 2021, pp. 1–4.
- [4] A. Bhandari, M. Feigin, S. Izadi, C. Rhemann, M. Schmidt, and R. Raskar, "Resolving multipath interference in kinect: An inverse problem approach," in *2014 IEEE SENSORS*, 2014, pp. 614–617.
- [5] A. Bhandari, A. Kadambi, R. Whyte, C. Barsi, M. Feigin, A. Dorrington, and R. Raskar, "Resolving multipath interference in time-of-flight imaging via modulation frequency diversity and sparse regularization," *Opt. Lett.*, vol. 39, no. 6, pp. 1705–1708, Mar 2014.
- [6] M. Ludwig and T. Loeliger, "3D ToF MPI multi-frequency mesh dataset," May 2023. [Online]. Available: <https://doi.org/10.5281/zenodo.7892452>